Nature of Molecular Interactions of Peptides with Gold, Palladium, and Pd–Au Bimetal Surfaces in Aqueous Solution

Hendrik Heinz,*,† Barry L. Farmer,‡ Ras B. Pandey,§ Joseph M. Slocik,‡
Soumya S. Patnaik,‡ Ruth Pachter,‡ and Rajesh R. Naik‡

Department of Polymer Engineering, University of Akron, Akron, Ohio 44325, Air Force Research Laboratory, Materials and Manufacturing Directorate, AFRL/RX, Wright-Patterson AFB, Ohio 45433, and Department of Physics and Astronomy, University of Southern Mississippi, Hattiesburg, Mississippi 39406

Received January 27, 2009; E-mail: hendrik.heinz@uakron.edu

Abstract: We investigated molecular interactions involved in the selective binding of several short peptides derived from phage-display techniques (8–12 amino acids, excluding Cys) to surfaces of Au, Pd, and Pd–Au bimetal. The quantitative analysis of changes in energy and conformation upon adsorption on even {111} and {100} surfaces was carried out by molecular dynamics simulation using an efficient computational screening technique, including 1000 explicit water molecules and physically meaningful peptide concentrations at pH = 7. Changes in chain conformation from the solution to the adsorbed state over the course of multiple nanoseconds suggest that the peptides preferably interact with vacant sites of the face-centered cubic lattice above the metal surface. Residues that contribute to binding are in direct contact with the metal surfaces, and less-binding residues are separated from the surface by one or two water layers. The strength of adsorption ranges from 0 to −100 kcal/(mol peptide) and scales with the surface energy of the metal (Pd surfaces are more attractive than Au surfaces), the affinity of individual residues versus the affinity of water, and conformation aspects, as well as polarization and charge transfer at the metal interface (only qualitatively considered here). A hexagonal spacing of ∼1.6 Å between available lattice sites on the {111} surfaces accounts for the characteristic adsorption of aromatic side groups and various other residues (including Tyr, Phe, Asp, His, Arg, Asn, Ser), and a quadratic spacing of ∼2.8 Å between available lattice sites on the {100} surface accounts for a significantly lower affinity to all peptides in favor of mobile water molecules. The combination of these factors suggests a "soft epitaxy" mechanism of binding. On a bimetallic Pd–Au {111} surface, binding patterns are similar, and the polarity of the bimetal junction can modify the binding energy by ∼10 kcal/mol. The results are semiquantitatively supported by experimental measurements of the affinity of peptides and small molecules to metal surfaces as well as results from quantum-mechanical calculations on small peptide and surface fragments. Interfaces were modeled using the consistent valence force field extended for Lennard-Jones parameters for fcc metals which accurately reproduce surface and interface energies [Heinz, H.; Vaia, R. A.; Farmer, B. L.; Naik, R. R. *J. Phys. Chem. C* **2008**, *112*, 17281–17290].

1. Introduction

A variety of inorganic−biological nanostructures and biomimetic materials with distinct functionalities can be assembled using nanoparticles of various chemical composition, peptide linkers, surfactants, and polymer matrices.[1−16] Peptides may regulate crystal growth of the inorganic material,[1,3−8,13] attract metal nanoparticles of a certain composition and size to form characteristic metal-coated wires,[3−5] assemble in predefined

† University of Akron.
‡ Air Force Research Laboratory.
§ University of Southern Mississippi.

(1) Brown, S.; Sarikaya, M.; Johnson, E. *J. Mol. Biol.* **2000**, *299*, 725–735.
(2) Wegner, G. J.; Lee, H. J.; Corn, R. M. *Anal. Chem.* **2002**, *74*, 5161–5168.
(3) Sarikaya, M.; Tamerler, C.; Jen, A. K. Y.; Schulten, K.; Baneyx, F. *Nat. Mater.* **2003**, *2*, 577–585.
(4) Fu, X. Y.; Wang, Y.; Huang, L. X.; Sha, Y. L.; Gui, L. L.; Lai, L. H.; Tang, Y. Q. *Adv. Mater.* **2003**, *15*, 902–906.
(5) Naik, R. R.; Jones, S. E.; Murray, C. J.; McAuliffe, J. C.; Vaia, R. A.; Stone, M. O. *Adv. Funct. Mater.* **2004**, *14*, 25–30.
(6) Gray, J. J. *Curr. Opin. Struct. Biol.* **2004**, *14*, 110–115.
(7) Slocik, J. M.; Stone, M. O.; Naik, R. R. *Small* **2005**, *1*, 1048–1052.
(8) Slocik, J. M.; Naik, R. R. *Adv. Mater.* **2006**, *18*, 1988.
(9) Xu, A.-W.; Ma, Y. R.; Colfen, H. *J. Mater. Chem.* **2007**, *17*, 415–449.
(10) Slocik, J. M.; Tam, F.; Halas, N. J.; Naik, R. R. *Nano Lett.* **2007**, *7*, 1054–1058.
(11) Chen, J.; Wiley, B. J.; Xia, Y. *Langmuir* **2007**, *23*, 4120–4129.
(12) Schiffrin, A.; Riemann, A.; Auwarter, W.; Pennec, Y.; Weber-Bargioni, A.; Cvetko, D.; Cossaro, A.; Morgante, A.; Barth, J. V. *Proc. Natl. Acad. Sci. U.S.A.* **2007**, *104*, 5279–5284.
(13) Grohe, B.; O'Young, J.; Ionescu, D. A.; Lajoie, G.; Rogers, K. A.; Karttunen, M.; Goldberg, H. A.; Hunter, G. K. *J. Am. Chem. Soc.* **2007**, *129*, 14946–14951.
(14) Jadzinsky, P. D.; Calero, G.; Ackerson, C. J.; Bushnell, D. A.; Kornberg, R. D. *Science* **2007**, *318*, 430–433.
(15) Heinz, H.; Vaia, R. A.; Farmer, B. L. *Langmuir* **2008**, *24*, 3727–3733.
(16) Cossaro, A.; Mazzarello, R.; Rousseau, R.; Casalis, L.; Verdini, A.; Kohlmeyer, A.; Floreano, L.; Scandolo, S.; Morgante, A.; Klein, M. L.; Scoles, G. *Science* **2008**, *321*, 943–946.

Report Documentation Page		*Form Approved* *OMB No. 0704-0188*

Public reporting burden for the collection of information is estimated to average 1 hour per response, including the time for reviewing instructions, searching existing data sources, gathering and maintaining the data needed, and completing and reviewing the collection of information. Send comments regarding this burden estimate or any other aspect of this collection of information, including suggestions for reducing this burden, to Washington Headquarters Services, Directorate for Information Operations and Reports, 1215 Jefferson Davis Highway, Suite 1204, Arlington VA 22202-4302. Respondents should be aware that notwithstanding any other provision of law, no person shall be subject to a penalty for failing to comply with a collection of information if it does not display a currently valid OMB control number.

1. REPORT DATE **2009**	2. REPORT TYPE	3. DATES COVERED **00-00-2009 to 00-00-2009**

4. TITLE AND SUBTITLE **Nature of Molecular Interactions of Peptides with Gold, Palladium, and Pd-Au Bimetal Surfaces in Aqueous Solution**	5a. CONTRACT NUMBER
	5b. GRANT NUMBER
	5c. PROGRAM ELEMENT NUMBER
6. AUTHOR(S)	5d. PROJECT NUMBER
	5e. TASK NUMBER
	5f. WORK UNIT NUMBER

7. PERFORMING ORGANIZATION NAME(S) AND ADDRESS(ES) **Department of Polymer Engineering,UniVersity of Akron,Akron,OH,44325**	8. PERFORMING ORGANIZATION REPORT NUMBER

9. SPONSORING/MONITORING AGENCY NAME(S) AND ADDRESS(ES)	10. SPONSOR/MONITOR'S ACRONYM(S)
	11. SPONSOR/MONITOR'S REPORT NUMBER(S)

12. DISTRIBUTION/AVAILABILITY STATEMENT
Approved for public release; distribution unlimited

13. SUPPLEMENTARY NOTES

14. ABSTRACT

15. SUBJECT TERMS

16. SECURITY CLASSIFICATION OF:			17. LIMITATION OF ABSTRACT	18. NUMBER OF PAGES	19a. NAME OF RESPONSIBLE PERSON
a. REPORT **unclassified**	b. ABSTRACT **unclassified**	c. THIS PAGE **unclassified**	**Same as Report (SAR)**	**11**	

Standard Form 298 (Rev. 8-98)
Prescribed by ANSI Std Z39-18

Table 1. Peptide Names, Binding Targets, and Amino Acid Sequences

name	binds to	peptide sequence[c]
A3	Au, Pd[a]	$^+$Ala-Tyr-Ser-Ser-Gly-Ala-Pro-Pro-Met-Pro-Pro-Phe$^-$
Flg—Na$_3$	Au, Pd[a]	$^+$Asp$^-$-Tyr-Lys$^+$-Asp$^-$-Asp$^-$-Asp$^-$-Asp$^-$-Lys^{+-} • 3 Na$^+$
Pd2—Cl	Pd[b]	$^+$Asn-Phe-Met-Ser-Leu-Pro-Arg$^+$-Leu-Gly-His-Met-His$^-$ • Cl$^-$
Pd4—Cl	Pd[b]	$^+$Thr-Ser-Asn-Ala-Val-His-Pro-Thr-Leu-Arg$^+$-His-Leu$^-$ • Cl$^-$
Flgd—Na$_2$		$^+$Asp$^-$-Tyr-Lys$^+$-Asp$^-$-Asp$^-$-Asp$^-$-Lys^{+-} • 2 Na$^+$
Gly10		Gly$_{10}$
Pro10		Pro$_{10}$

[a] References 7, 8. [b] These peptide sequences from phage display are newly reported here. [c] The approximation of the charge state equivalent to pH = 7 in the models is indicated.

nanoscale patterns,[12] and influence optical properties of the inorganic nanostructures.[2,10,11] For example, the plasmon resonance frequency of metal nanorods depends on the size and shape of the nanoparticles as well as on the presence of molecular recognition groups, such as peptides or surfactants attached to the surface. In this configuration, binding of an external agent to surface-attached peptides can induce sufficient shifts in UV/vis absorption to support sensor capabilities.[2]

A major challenge lies in the tremendous number of potential peptides and lack of control over binding affinities. For example, given a pool of 20 natural amino acids to assemble a 12-peptide, there are $N = 20^{12} = 10^{15.6}$ different potential peptides. The screening of all peptides is currently impossible; however, phage display techniques allow researchers to identify peptide sequences with specific binding affinity to nanoparticles and surfaces.[1,3,5—8,17—19] In this procedure, commercial libraries of several billion phages with distinct peptide sequences expressed at the PIII minor coat protein were screened on various surfaces of gold, palladium, and silver nanoparticles, as well as on surfaces of montmorillonite, silica, germanium oxide, tin oxide, titania, and zinc oxide.[5,8] After incubation of the entire library of phages, including the displayed peptides of typically 8—12 amino acid length, with the nanoparticles in solution, and after several washing cycles with HEPES buffer solution near pH = 7, the most strongly binding peptides remain bound to the inorganic surfaces. These sequences have been identified by analysis of the corresponding phage DNA (some shown in Table 1).[6] The relative binding strength, transmission electron microscopy (TEM), IR spectroscopy, NMR spectroscopy, and thermochemical data were recorded to characterize the peptide-modified nanoparticles in comparison to the peptides in solution.[1—13,17—19]

The molecular reasons for highly specific binding in the absence of thiol groups in the peptides, however, have remained largely a matter of speculation. Several studies attempted an explanation on the basis of experimental[1,3—13,17—20] and simulation data;[21—31] however, evidence about the acting mechanisms is often vague, and modeling studies often employed excessively crude approximations. We present the first steps using molecular simulation as a tool to understand the reasons for binding of
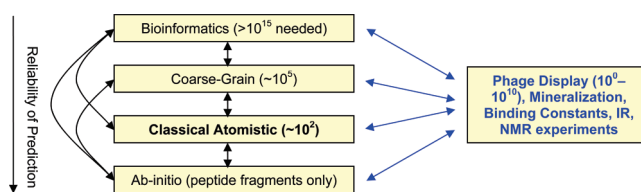
Figure 1. Modeling peptide—surface interactions and biological self-assembly using techniques at various levels. The currently distinguishable number of dodecapeptides for each technique is indicated in parentheses. We focus on classical atomistic simulation in comparison with experiment and simulation at other levels.

selected experimental and control peptide sequences, including the computation of adsorption energies, changes in peptide conformation upon adsorption, and the strength of interaction of amino acid residues upon interaction with the surface in aqueous solution (Figure 1). In contrast to earlier work, our approach includes an accurate representation of metal surface energies[32—36] using a Lennard-Jones model for face-centered cubic (fcc) metals compatible with various force fields,[29] considers the dynamics on the time scale of nanoseconds at 298 K as opposed to static calculations at 0 K, and involves approximately 1000 water molecules as opposed to unspecific implicit water models, few static water molecules, or no water molecules at all. Therefore, temperature, pH, and ionic concentration are tangible quantities in the simulation. We also benefit from an efficient new method for the computation of binding energies for the peptides. The viability of this approach is supported by recent improvements in the accuracy of force field parameters for inorganic components[29,37—41] and the identification of polarization effects on metal surfaces[42—46] as modest contributions.

(17) Willett, R. L.; Baldwin, K. W.; West, K. W.; Pfeiffer, L. N. *Proc. Natl. Acad. Sci. U.S.A.* **2005**, *102*, 7817–7822.
(18) Roach, P.; Farrar, D.; Perry, C. C. *J. Am. Chem. Soc.* **2005**, *127*, 8168–8173.
(19) Zorbas, V.; Smith, A.; Xie, H.; Ortiz-Acevedo, A.; Dalton, A. B.; Dieckmann, G. R.; Draper, R. K.; Baughman, R. H.; Musselman, I. H. *J. Am. Chem. Soc.* **2005**, *127*, 12323–12328.
(20) Li, Z.; Calaza, F.; Gao, F.; Tysoe, W. T. *Surf. Sci.* **2007**, *601*, 1351–1357.
(21) Haftel, M. I.; Bernstein, N.; Mehl, M. J.; Papaconstantopoulos, D. A. *Phys. Rev. B* **2004**, *70*, 125419:1–15.
(22) Vassilev, P.; van Santen, R. A.; Koper, M. T. M. *J. Chem. Phys.* **2005**, *122*, 054701.
(23) Oren, E. E.; Tamerler, C.; Sarikaya, M. *Nano Lett.* **2005**, *5*, 415–419.
(24) Schravendijk, P.; van der Vegt, N.; Delle Site, L.; Kremer, K. *ChemPhysChem* **2005**, *6*, 1866–1871.
(25) Kantarci, N.; Tamerler, C.; Sarikaya, M.; Haliloglua, T.; Doruker, P. *Polymer* **2005**, *46*, 4307–4313.
(26) Schravendijk, P.; Ghiringhelli, L. M.; Delle Site, L.; van der Vegt, N. F. A. *J. Phys. Chem. C* **2007**, *111*, 2631–2642.
(27) Miao, L.; Seminario, J. M. *J. Phys. Chem. C* **2007**, *111*, 8366–8371.
(28) Ghiringhelli, L. M.; Delle Site, L. *J. Am. Chem. Soc.* **2008**, *130*, 2634–2638.
(29) Heinz, H.; Vaia, R. A.; Farmer, B. L.; Naik, R. R. *J. Phys. Chem. C* **2008**, *112*, 17281–17290.
(30) Pandey, R. B.; Heinz, H.; Feng, J.; Farmer, B. L.; Slocik, J. M.; Drummy, L. R.; Naik, R. R. *Phys. Chem. Chem. Phys.* **2009**, *11*, 1989–2001.
(31) Hong, G.; Heinz, H.; Naik, R. R.; Farmer, B. L.; Pachter, R. *ACS Appl. Mat. Interf.* **2009**, *1*, 388–392.
(32) Tyson, W. R.; Miller, W. A. *Surf. Sci.* **1977**, *62*, 267–276.
(33) Menon, S. K.; Martin, P. L. *Ultramicroscopy* **1986**, *20*, 93–98.
(34) Flueli, M.; Borel, J. P. *J. Cryst. Growth* **1988**, *91*, 67–70.
(35) *CRC Handbook of Chemistry and Physics*, 84th ed.; Lide, D. R., Ed.; CRC Press: Boca-Raton, FL, 2003.
(36) Osman, M. A.; Keller, B. A. *Appl. Surf. Sci.* **1996**, *99*, 261–263.
(37) Heinz, H.; Castelijns, H. J.; Suter, U. W. *J. Am. Chem. Soc.* **2003**, *125*, 9500–9510.
(38) Heinz, H.; Suter, U. W. *J. Phys. Chem. B* **2004**, *108*, 18341–18352.
(39) Heinz, H.; Suter, U. W. *Angew. Chem., Int. Ed.* **2004**, *43*, 2239–2243.
(40) Heinz, H.; Koerner, H.; Vaia, R. A.; Anderson, K. L.; Farmer, B. L. *Chem. Mater.* **2005**, *17*, 5658–5669.
(41) Heinz, H.; Vaia, R. A.; Farmer, B. L.; Heinz, H.; Vaia, R. A.; Farmer, B. L. *J. Chem. Phys.* **2006**, *124*, 224713.
(42) Bardeen, J. *Phys. Rev.* **1940**, *58*, 727–736.
(43) Lang, N. D.; Kohn, W. *Phys. Rev. B* **1973**, *7*, 3541–3550.
(44) Smith, N. V.; Chen, C. T.; Weinert, M. *Phys. Rev. B* **1989**, *40*, 7565–7573.
(45) Finnis, M. W. *Surf. Sci.* **1991**, *241*, 61–72.

Therefore, semiempirical classical simulation in close relation to experiment and other theoretical approaches can provide insight into the nature of molecular interactions at such inorganic−organic interfaces (Figure 1). We limit the investigation to well-defined even {111} and {100} surfaces; the influence of the shape and composition of the nanoparticles shall be considered elsewhere. Further background information on simulation methods can be found in section S1 of the Supporting Information.

The paper is organized as follows. In section 2, we describe the peptide sequences and summarize the computational approach. Sections 3 and 4 are dedicated to the presentation of simulation results on even monometallic surfaces and on bimetallic surfaces. Section 5 focuses on the comparison of results to experiment and explains our hypothesis of the specificity and strength of peptide interactions with metal surfaces. A summary is presented in section 6. The Supporting Information includes a description of the computational screening approach (S2), simulation protocols (S3), and additional evidence on the binding mechanism from earlier simulations (S4).

2. Peptide Sequences and Computational Details

2.1. Sequence of the Peptides. We have chosen four peptides named A3, Flg−Na$_3$, Pd2−Cl, Pd4−Cl, which were identified as the strongest metal-binding peptides from a pool of ∼10^9 peptides by phage display.[7,8] The neutral peptide A3 and the three-fold negatively charged peptide Flg−Na$_3$ at pH = 7 have shown affinity to Au and Pd nanoparticles. The peptides Pd2−Cl and Pd4−Cl are newly reported here and have shown affinity to Pd nanoparticles. For comparison, we also include the peptide Flgd−Na$_2$, deficient in one Asp residue compared to Flg−Na$_3$, as well as the arbitrarily chosen peptides Gly10 and Pro10 of unknown specificity of adsorption (Table 1). We assume pH = 7, which is characterized by protonation or deprotonation of the corresponding amino acid side chains according to their pK_a values, including a zwitterionic structure of the peptides with a protonated N-terminal end and a carboxylate C-terminal end. For amino acids whose charges do not compensate to zero within the peptide, equivalent amounts of counterions Cl$^−$ or Na$^+$ are added to maintain charge neutrality.

2.2. Efficient Computation of Adsorption Energies. The quantitative computation of adsorption energies requires the inclusion of explicit water molecules and ionic solutes due to the formation of spatially oriented hydrogen bonds which change their orientation when peptides (or other adsorbates) move from the solution to the surface. We utilize a new, efficient approach which involves the simulation of four systems, (1) the surface-solute−solvent system of average energy E_1, (2) the solute−solvent system of average energy E_2, (3) the solvent system of average energy E_3, and (4) the surface-solvent system of energy E_4 under consideration of equal molecular volumes for each component under NVT conditions. The adsorption energy is calculated from the average energy of each of the four systems as $E_{ads} = E_1 - E_2 + E_3 - E_4$. Each simulation requires an accurate summation of Coulomb interactions on the order of ≤0.1 kcal/mol uncertainty for the entire system as well as precise temperature control or energy corrections to a reference temperature, respectively. Details can be found in section S2 of the Supporting Information.

2.3. Models, Force Field Parameters, and Simulation Protocol. Fully atomistic models of the peptides, metal surfaces, and water were prepared using the Hyperchem[47] and Materials Studio Visualizers.[48] Box dimensions were typically 3 nm × 3 nm × z whereby the additive box height z amounts to ≥1.2 nm for metal
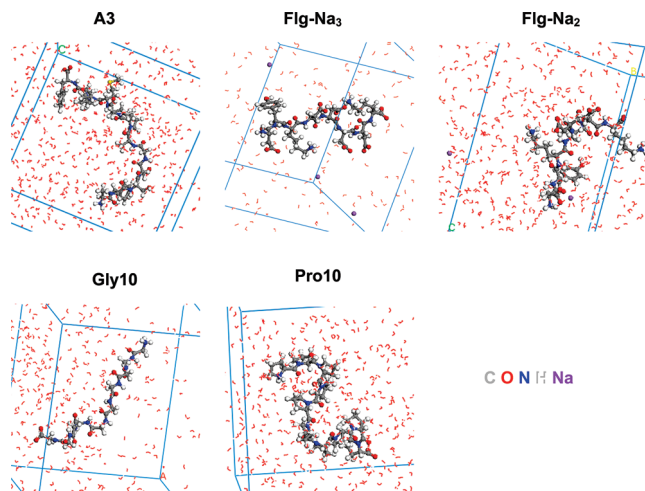

Figure 2. Representative snapshots of the peptides in solution. The peptides A3, Flg−Na$_3$, and Flgd−Na$_2$ assume unspecific 3D conformations, and a tendency toward intramolecular interactions between the charged −CO$_2$$^−$ groups and H$_3$N$^+$/Na$^+$ ions is seen for Flg−Na$_3$ and Flgd−Na$_2$. The peptide Gly10 prefers an extended conformation and is conformationally very flexible. Polyproline Pro10 assumes a helical structure.

substrates, and to ≥3.5 nm for water and aqueous solutions of the peptides. The size was chosen such that 25% to 40% of the surface area is covered by the peptide, close to experimental conditions. The consistent valence force field (CVFF)[48,49] extended for accurate Lennard-Jones parameters for fcc metals[29] was employed in the simulation of the metal-water−peptide hybrid systems. The parameters for fcc metals reproduce surface energies and interface energies in quantitative agreement with experiment (1−10%), down from deviations up to 500% in earlier force fields. The Discover program[48] as well as LAMMPS[50] were employed to carry out molecular dynamics simulations. Models, force field, simulation protocols, and accuracy are described in section S3 of the Supporting Information.

3. Adsorption of Peptides on Even {111} and {100} Surfaces of Au and Pd

The peptides were relaxed in aqueous solution (Figure 2) and on the metal {111} and {100} surfaces (Figure 3) by molecular dynamics simulation. Corresponding adsorption energies (Table 2) indicate that peptides are generally attracted to the metal surfaces, supported by the observation of direct contact with the metal surface or the presence of one or two water interlayers in the models (Figure 3). The order of magnitude of computed binding energies for the oligopeptides, between 0 and −100 kcal/mol, is in the range of noncovalent interactions (<100 kcal/mol) and often stronger than that of a simple collection of hydrogen bonds (1−4 kcal/mol). The adsorption strength correlates with the amount of direct contact with the metal surface and differs significantly between the {111} and the {100} surfaces. In the peptides, we can identify binding residues versus nonbinding residues. Strongly binding peptides contain several binding residues, while the remaining residues are less-binding or nonbinding. In Flgd−Na$_2$, the elimination of a single amino acid (Asp) in the peptide sequence compared to Flgd−Na$_3$ leads to a modest reduction in binding strength (Table 2).

(46) Guidelli, R.; Schmickler, W. *Electrochim. Acta* **2000**, *45*, 2317–2338.
(47) *HyperChem 7.5*; Hypercube Inc.: Gainesville, FL, 2006.
(48) *Materials Studio 4.0*, Discover Program, Cerius2, and User Guide; Accelrys, Inc.: San Diego, CA, 2005.

(49) Dauber-Osguthorpe, P.; Roberts, V. A.; Osguthorpe, D. J.; Wolff, J.; Genest, M.; Hagler, A. T. *Proteins: Struct., Funct. Genetics* **1988**, *4*, 31–47.
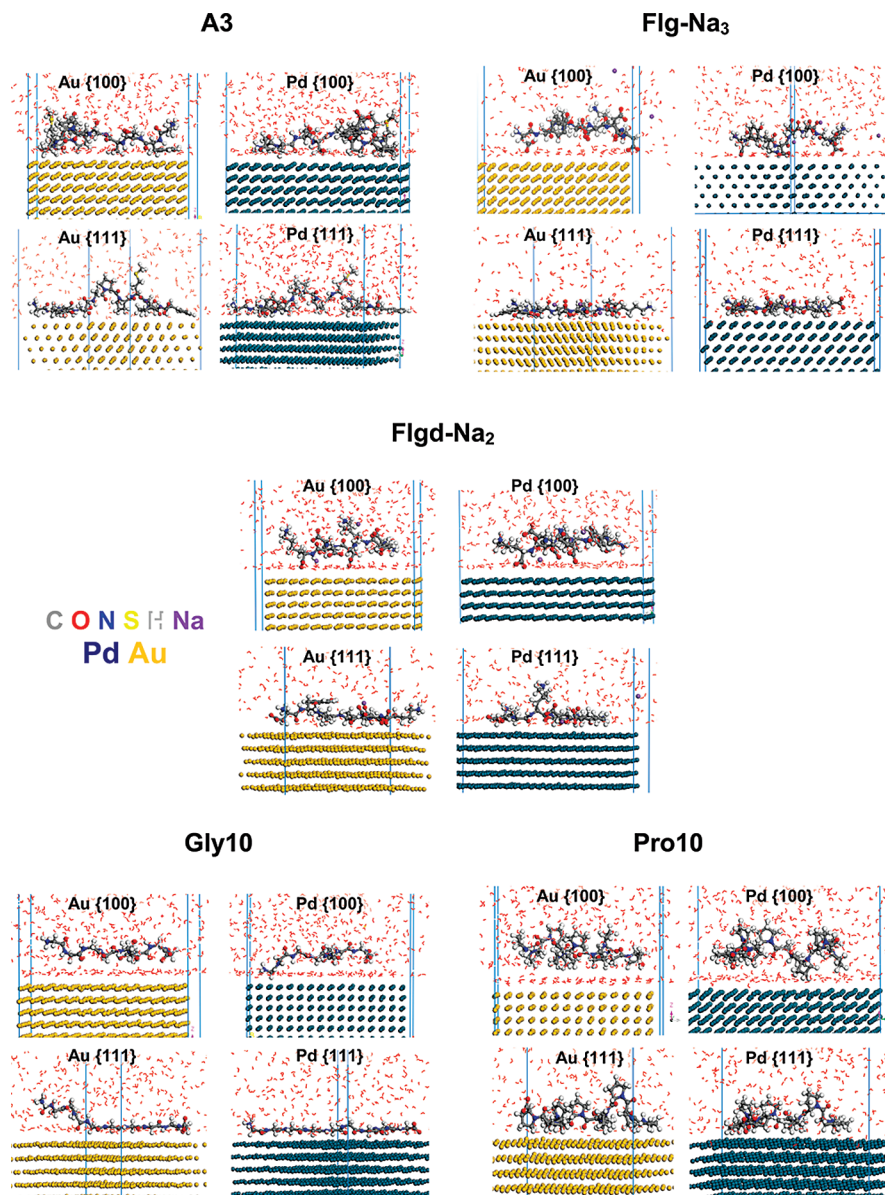(50) Plimpton, S. J. *J. Comp. Phys.* **1995**, *117*, 1–19.

Figure 3. Representative snapshots of the peptides A3, Flg−Na$_3$, Flgd−Na$_2$, Gly10, and Pro10 on the metal surfaces, viewed along different perspectives to support a spatial impression. Some counterions are not shown due to diffusion out of the displayed region.

3.1. Direct Contact to the Metal Surface and Adsorption Strength. We define direct contact as a distance of the atoms of residues or chain fragments ≤3 Å from the metal surface atomic plane for the majority of the time, with typical distances of 2.5 Å. In cases of strong binding, individual side groups or backbone residues are found in direct contact with the metal surface, without intermediate water molecules between the peptide and the metal surface (Figure 3). In cases of weak binding, there is no such direct contact, and multiple "layers" of water molecules accumulate between the metal surface and the peptide. For a single water layer in between, the atoms of the residues or chain fragments nearest to the metal surface atomic plane are typically found within a distance of 5 Å for the majority of the time. For multiple water layers in between, the average distance is accordingly greater.

For all peptides, adsorption is stronger on the {111} surface compared to the {100} surface. The adsorption energy on {100} surfaces amounts only to ∼10% compared to {111} surfaces for the peptides A3 and Flg−Na$_3$. The control peptide Gly10

also shows a strong adsorption on {111} surfaces and high selectivity. The control peptide Pro10 is the least binding peptide in all instances, although moderate attraction is also seen to {111} surfaces. The visualization supports that oligoprolines may be suitable to form loops to connect more specialized peptide fragments (Figures 2 and 3). In binding peptides, at least a few binding amino acids, groups of amino acids, or the entire peptide are in direct contact with the metal surface for most of the time, which accounts for the majority of the binding energy. The correlation between independent conformations of the same peptide and corresponding adsorption energies further indicates cooperativity between adjacent amino acids: the presence of less-binding residues near binding residues in the peptide chain as well as the polymerization of individually less strongly binding residues to homopeptides (Gly10, Pro10) can increase the extent of direct contact with the surface and the overall binding energy.

3.2. Amino-Acid-Specific Contributions to Adsorption Strength. Analysis of the MD trajectories provides the first amino-acid-specific trends to guide in the design of peptides

Table 2. Adsorption Energies of the Peptides, in kcal/mol (±5 kcal/mol or up to ±10%), and a Compilation of Residues in Direct Contact with the Surface[a]

metal surface	peptide				
	A3	Flg−Na$_3$	Flgd−Na$_2$	Gly10	Pro10
Au {100}	−9	0	−6	−4	0
	$_2$Tyr, $_4$Ser, $_8$Pro (partly), $_9$Met (main chain), $_{10}$Pro	2 CO$_2^-$ of Asp	2 CO$_2^-$ of Asp and $_7$Lys	none	none
Au {111}	−63	−63	−45	−60	−23
	first five residues $_1$Ala−$_2$Tyr−$_3$Ser−$_4$Ser−$_5$Gly, $_8$Pro (partial), $_{11}$Pro, and $_{12}$Phe (incl. CO$_2^-$)	all residues; $_2$Tyr, 1−2 CO$_2^-$ of $_{1,4−7}$Asp, $_8$Lys partly detached; Na$^+$ −CO$_2^-$ bridges	$_1$Asp and $_3$Lys to $_7$Lys; NH$_3^+$ of $_1$Asp, $_{3,7}$Lys and 1−2 CO$_2^-$ of Asp partly detached	6−7 consecutive Gly residues	2−3 Pro and additional partial contacts
Pd {100}	−2	+3	+4	−27	−13
	$_1$Ala, $_2$Tyr, $_4$Ser, $_8$Pro (partly), $_9$Met (main chain), and $_{10}$Pro	1−2 CO$_2^-$ of Asp and $_3$Lys	NH$_3^+$ of $_1$Asp, CO$_2^-$ on $_7$Lys, sometimes CO$_2^-$ of Asp	1−2 Gly residues	1 Pro (partial) and CO$_2^-$ of $_{10}$Pro (partial)
Pd {111}	−77	−85	−60	−75	−40
	first five residues $_1$Ala−$_2$Tyr−$_3$Ser−$_4$Ser−$_5$Gly, $_8$Pro (partial), $_{11}$Pro, and $_{12}$Phe	all residues; NH$_3^+$ of $_1$Asp, $_{3,8}$Lys, and 1−2 CO$_2^-$ (Asp) less attached, Na$^+$−CO$_2^-$ bridges	all residues except $_3$Lys; 1 CO$_2^-$ of Asp and NH$_3^+$ of $_1$Asp partly detached	7−9 residues incl. CO$_2^-$ of $_{10}$Gly	5−6 Pro and additional partial contacts

[a] The subscript to the left indicates amino acid positions within the peptide.
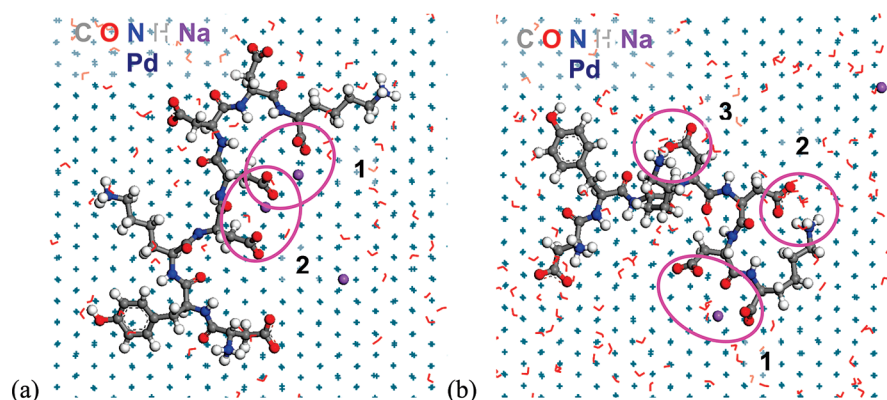
Figure 4. Top view of representative snapshots of (a) Flg−Na$_3$ and (b) Flgd−Na$_2$ on a Pd {111} surface. (a) In Flg−Na$_3$, all residues are in direct contact with the surface, and ions pairs (1 and 2) are highlighted. (b) Flgd−Na$_2$ contains one Asp residue less and forms different internal ion pairs (1−3). The side chain of $_3$Lys in feature 3 is detached from the surface.

(Table 2).[51] In A3, the phenyl groups in $_2$Tyr and $_{12}$Phe attach preferably to the planar {111} Pd surface, interconnected by less tightly bound Ala, Pro, and Met residues. On the Au {111} surface, the phenyl ring of $_{12}$Phe is less tightly bound compared to that on the Pd {111} surface. The exact analysis of the adsorption energy of individual residues is challenging due to changes in solvation and conformation upon contact with the surface. Nevertheless, the two aromatic units and their surrounding region in the peptide chain can be regarded as anchoring residues and account for much of the binding energy. This view concurs with a less intense adsorption of A3 on the Au {111} surface compared to the Pd {111} surface. Direct contact with fewer residues of A3 is observed on the Pd {100} and Au {100} surfaces (Table 2). The adsorption strength of the individual amino acids is also significantly weaker.

In Flg−Na$_3$, all residues of the peptide are in direct contact with the Pd {111} surface, mostly driven by the $_2$Tyr residue as well as 3−4 CO$_2^-$ groups of $_{1,4−7}$Asp and the C-terminal $_8$Lys (Figure 4a). The $_{3,8}$Lys side chains and 1−2 CO$_2^-$ groups

are not in direct contact for part of the time. Notable are intramolecular bridges between Na$^+$ ions and CO$_2^-$ groups (features 1 and 2). On the Au{111} surface, the adsorption geometry is similar except for somewhat reduced contact with $_2$Tyr and lower adsorption energy. On the Pd and Au {100} surfaces, one or two CO$_2^-$ groups of the Asp residues or $_3$Lys are in contact with the metal surface, yet essentially no adsorption results.

In Flgd−Na$_2$, all groups except $_3$Lys directly interact with the Pd {111} surface (Figure 4b). Complexes between a sodium ion with CO$_2^-$ groups can be seen (feature 1); the other sodium ion floats at a distance in solution. $_7$Lys coordinates with $_5$Asp (feature 2), and $_3$Lys coordinates with $_4$Asp (feature 3). On the Au {111} surface, $_2$Tyr is not in contact with the surface, while the rest of the peptide including $_3$Lys is bound. The binding strength is mainly associated with CO$_2^-$ groups in Asp and $_7$Lys and sometimes another CO$_2^-$ group of $_6$Asp. The adsorption is weaker compared to that on Pd {111}, even though the amount of direct contact is similar. Less contact is seen on the Au and Pd {100} surfaces (Table 2), and the adsorption is small to negligible.

(51) A systematic study of the adsorption of single amino acids on a metal surface in solution will be reported separately.

The reference peptides Gly10 and Pro10 also exhibit interesting trends. Most notably, the binding potential of Gly10 is high. Seven to nine Gly residues, including the C-terminal CO_2^- group, bind to Pd {111}, and some residues including $_6$Gly near the center of the chain favor a water interlayer and detach from the surface (Figure 3). Six or seven consecutive Gly residues toward the C-terminal end bind to Au {111}, and the adsorption energy is close to that of A3 and Flg−Na3. Also, the Pd {100} surface attracts a few Gly residues, while Au {100} shows no adsorption.

Pro10 is essentially inert against the Au {100} surface and shows some adsorption through two or three Pro residues on the Au {111} surface. It interacts slightly with Pd {100}, which results in minor adsorption, and substantially with Pd {111} through five or six residues and other partial contacts, including the C-terminal CO_2^- group. However, the proline helix resists flattening so that the adsorption energy remains less than half the value compared to other peptides.

3.3. Differences in Secondary Structure upon Adsorption.

Adsorption of the peptides is also related to differences in solvation in the presence of the surface compared to the state in solution. The peptides are short but of a critical length to observe secondary structure formation.

Peptide A3 in solution is of a nonspecific, flexible conformation which essentially converts into a flat-on (2D) structure in the presence of {111} surfaces. A few residues close to Pro in the middle section of the peptide are not directly bound and retain flexibility. On the {100} surfaces, the peptide exhibits a 3D structure closer to the solution state. Peptide Flg−Na$_3$ in solution forms intramolecular $-CO_2^- \cdots H_3N^+-$ bridges between $_8$Lys and $_{5,4}$Asp as well as between $_3$Lys and $_{6,7}$Asp, which lead to a 3D shaped (and concentration-dependent) conformation (Figure 2). On the {111} surfaces, these intramolecular bridges are given up in favor of a flat-on, 2D shape which involves several $CO_2^- \cdots Na^+$ bridges (Figure 4a). On the less attractive {100} surfaces, more 3D features are preserved. Peptide Flgd−Na$_2$, missing one Asp residue compared to Flg−Na$_3$, exhibits less intramolecular bridging in solution. Upon adsorption on the {111} surfaces, it approaches a 2D backbone except for one or two residues, supported by stabilizing ion pairs (Figure 4b). The solution structure is also preserved to a higher extent on the {100} surfaces. Peptide Gly10 in solution prefers an extended conformation with significant conformational flexibility (Figure 2). Upon adsorption, the peptide appears mostly "glued" to the Pd {111} surface, less so to the Au {111} surface, and maintains significant conformational flexibility on the {100} surfaces (Figure 3). Peptide Pro10 in solution forms a mixture of polyproline II and polyproline I helices due to the steric demand of the pyrrolidine rings (Figure 2). Upon adsorption, the conformation is biased toward contact with the surface. Particularly on Pd {111}, more than half the residues are in contact with the surface, less so on Au {111}. Minor contacts are seen on the Pd {100} surface and no contact with the Au {100} surface (Table 2).

Significant conformational changes such as a bias toward 2D structures and greatly reduced mobility of individual groups on {111} surfaces upon adsorption indicate a significant loss in entropy. While it is time-consuming to quantify the entropy balance computationally, a crude estimate can be based on loss in rotational degrees of freedom of the peptide and an increase in lateral mobility of bound water such as during a melting transition. The assumption of four rotatable bonds with three equal rotational states each per amino acid (main chain +

Table 3. Data on the Polarity of Pd−Au Interfaces for Use in an Extended Born Model,[38] in MJ/mol

property	Pd	Au
sublimation energy[a]	0.38	0.37
first ionization energy[a]	0.80	0.89
second ionization energy[a]	1.88	1.98
first electron affinity[a]	*0.054*	*0.223*
enthalpy of alloy formation[b]	$-0.02 < \Delta H < 0$	

[a] Reference 35. [b] References 52−54.

average side chain) for a 10-peptide results in a conformational entropy of $S = 10k \ln 3^4$, equal to a maximum loss in entropic freedom of $-T\Delta S \approx 40kT \approx 24$ kcal/mol. The concomitant release of 25 water molecules, which approximately corresponds to the surface area covered by an extended 10-peptide, results in a maximum entropy increase of $25\Delta S_f$, where ΔS_f corresponds to the fusion entropy[35] and leads to $-S\Delta T = -39$ kcal/mol. We observe in the simulation that certainly not all degrees of freedom are lost, particularly so for bound water molecules, so that actual values may be less than half of the maximum and significantly compensate each other. Therefore, computed binding energies in Table 2 are likely acceptable approximations of binding free energies as well.

4. Adsorption of Peptides on a Bimetallic Pd{111}−Au{111} Interface

We further analyzed the adsorption of the peptides A3, Flg−Na$_3$, Flgd−Na$_2$, Pd2Cl, and Pd4Cl on even bimetallic Pd−Au {111} surfaces with a smooth, idealized boundary between Pd and Au. The boundary creates an electrostatic potential difference between the two metals, and the method of Heinz and Suter[38] was employed for an estimate of the polarity, since quantitative experimental data were not available.

4.1. Polarity of the Bimetal Interface.

The ground-state electron configurations of Pd and Au are [Pd] $5s^0 4d^{10}$ and [Au] $6s^1 4f^{14} 5d^{10}$, in which the partially occupied 6s orbital of Au indicates its action as an electron acceptor. Atomization and ionization energies confirm this trend and permit an estimate of the atomic charges at the interface using an extended Born model (Table 3).[38] The enthalpy of alloy formation, and therefore the enthalpy of formation of the Pd−Au interface, is close to zero.[52−54] The analysis for different atomic charges ($\pm 0e$, $\pm 0.5e$, $\pm 1.0e$, $\pm 2.0e$) in a bulk mixture and for a single flat interface suggests a polarity near $\pm 1e$ in a 3D bulk alloy and near $\pm 0.3e$ at a 2D flat interface (Figure 5).

While we note a significant difference in atomic charges between a bulk mixture and a smooth interface, we employ charges of $+0.3e$ for Pd and $-0.3e$ for Au atoms ($\pm 0.1e$) at the flat interface (all other metal atoms $\pm 0.0e$). The assignment agrees with X-ray measurements of the electron deformation density of reference structures of the form A_1B_1.[38]

4.2. Trends in Adsorption Energies.

We computed the adsorption energy of the peptides on the Pd−Au {111} bimetallic surface (Table 4). The presence of distinct surface areas of Au and Pd allowed monitoring the preferred location of the peptides in the course of the simulation (Figure 6). Different start positions were chosen arbitrarily between the Au and Pd surface which do not affect the final result after sufficient

(52) Tayler, J. B. *Proc. Phys. Soc. London* **1899**, *17*, 194–201.
(53) Niessen, A. K.; de Boer, F. R.; Boom, R.; de Chatel, P. F.; Mattens, W. C. M. *CALPHAD* **1983**, *7*, 51–70.
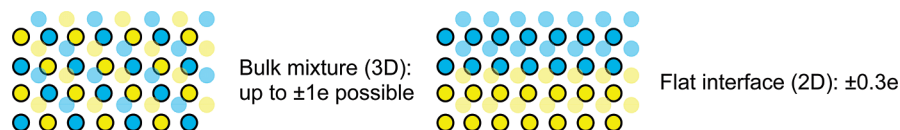(54) Meschel, S. V.; Kleppa, O. J. *J. Alloys Compd.* **2003**, *350*, 205–212.

Figure 5. Estimate of atomic charges at Pd−Au interfaces. Compared to (a) a 3D homogeneous distribution, (b) a flat interface leads to less efficient charge transfer. The gain in Coulomb energy per charged atom amounts only to 1/8 for the same atomic charges.

Table 4. Adsorption Energies at the Pd−Au {111} Bimetal Surface, in kcal/mol per Peptide (±5 kcal/mol or up to ±10%), and a Compilation of Residues in Direct Contact with the Surface

	metal surface		
peptide	Pd−Au {111}	Pd {111}	Au {111}
A3	−86	−77	−63
	most of $_1$Ala to $_6$Ala, $_8$Pro and $_{10}$Pro (partly), $_{11}$Pro and $_{12}$Phe		
Flg−Na$_3$	−74	−85	−63
	all residues, except sometimes NH$_3^+$ of $_1$Asp, side chains in 1−2 Asp and in $_{3,8}$Lys		
Flgd−Na$_2$	−63	−60	−45
	$_1$Asp, $_2$Tyr, $_4$Asp to $_7$Lys, side chains in 1−2 residues (Asp, $_7$Lys) sometimes detached, ion pair between $_3$Lys and $_6$Asp		
Pd2−Cl	−78		
	all residues; $_1$Asn incl. NH$_3^+$, $_3$Met, $_5$Leu, $_9$Gly, and $_{12}$His incl. CO$_2^-$ sometimes detached		
Pd4−Cl	−93		
	all residues except $_7$Pro; $_5$Val, $_8$Thr, $_9$Leu, and $_{12}$Leu sometimes detached		

simulation time. In some cases, lateral offset of the peptide and continued simulation on the order of several nanoseconds were required to identify energetically preferred locations. All peptides remain spatially flexible and gravitate toward the Pd domain of the surface. Due to polarity, the Pd−Au bimetal interface acts as a preferred adsorption site for A3 and lowers the (negative) adsorption energy further by about 10 kcal/mol in comparison to the most attractive monometallic {111} surface. However, less attraction is observed for charged Flg−Na$_3$ (Table 4). In every case, adjustments in conformation of the peptide backbone occur to adapt to the polarity of the Pd−Au interfacial region. Patterns of binding and less-binding residues are similar to those observed on monometallic surfaces, and the adsorption strength is of similar magnitude. In Pd2−Cl and Pd4−Cl, Phe, His, Arg, and Asn are the most strongly binding residues.

Peptide A3 translates to the Pd−Au interface in the initial stages of the simulation and remains there for the rest of the time. Almost the entire peptide is in direct contact with the metal surface, and the adsorption strength is increased relative to that observed on Pd {111} and Au {111} surfaces. The orientation of polar functional groups in the backbone and in the side chains complementary to the polar Pd$^{+0.3}$···Au$^{-0.3}$ interface may account for this effect, for example, −NH−, −OH groups of $_2$Tyr and $_3$Ser near interfacial Au, and carbonyl oxygen atoms of $_{10,11}$Pro near interfacial Pd (Figure 6). Peptide Flg−Na$_3$ also prefers the Pd domain, and all residues assume direct contact with the metal similar to the observation on the Pd {111} surface. However, a reduction in adsorption strength by ca. 10 kcal/mol was found. For example, CO$_2^-$ groups of $_{1,6}$Asp and $_8$Lys are found near interfacial Pd (+0.3e), and −NH$_3^+$ and −OH of $_3$Lys and $_2$Tyr are found in the vicinity of interfacial Au (−0.3e). The peptide Flgd−Na$_2$ is also attracted to the Pd domain of the surface, and similar characteristic orientation of polar groups along the Pd−Au interface is seen (Figure 6).

The peptide Pd2−Cl exhibits an extended conformation and no intramolecular ion pairs in solution. On the Pd−Au bimetal {111} surface, the entire peptide is in direct contact with the surface and adsorbs strongly with −78 kcal/mol. Simulation with different start structures indicates that the residues $_1$Asn,

$_2$Phe, $_7$Arg, and $_{10,12}$His contribute particularly to adsorption. A preference for the Pd domain of the bimetal surface is noticed, and the polarity of the Pd−Au interface supports the adsorption of some residues in its vicinity (Figure 6). The peptide Pd4−Cl is also of an extended conformation in solution without intramolecular ion pairs. Upon adsorption, direct contact with the bimetal is made through all residues but $_7$Pro. Hydrophobic residues are partly detached from the surface (Table 4), and the adsorption energy is very high at −93 kcal/mol, even though the peptide extends across Pd and Au domains. Simulations with different start structures indicate that $_3$Asn, $_{6,11}$His, and $_{10}$Arg, as well as $_{1,8}$Thr, contribute particularly to adsorption.

5. Comparison with Experiment and Binding Mechanism

The simulation provides semiquantitative measures of adsorption energies and insight into the rich interplay of factors that contribute to binding. Nevertheless, we need to consider limitations of the model. We neglect contributions due to polarization and charge transfer at the metal interface (covalent bonding contributions), finite-size effects owed to limitations in box size to 3−5 nm and application of periodic boundary conditions, shortcomings of the force field models, and the existence of other peptide conformations which may not have been captured due to long relaxation times on the metal surfaces. Yet the body of results is consistent with numerous experimental data and permits substantial conclusions on the mechanism of binding as discussed in the following.

5.1. Experimental Evidence for Adsorption of Peptides on Pd, Au, and Pd−Au Bimetal Surfaces. Brown et al.[1] identified noncovalent adhesion of peptides to Au {111} faces by protein-induced growth of Au nanocrystals. Fu et al.[4] observed the adsorption of Pd and Au nanoparticles of 4−5 nm average size onto a fibrillar dodecapeptide (T1, Arg-Gly-Tyr-Phe-Trp-Ala-Gly-Asp-Tyr-Asn-Tyr-Phe). The metal particles were obtained by reduction of PdCl$_2$ and HAuCl$_4$ in solution, which typically leads to {111} surfaces. The high content of aromatic residues Tyr, Phe, and Trp in peptide T1 was associated with strong
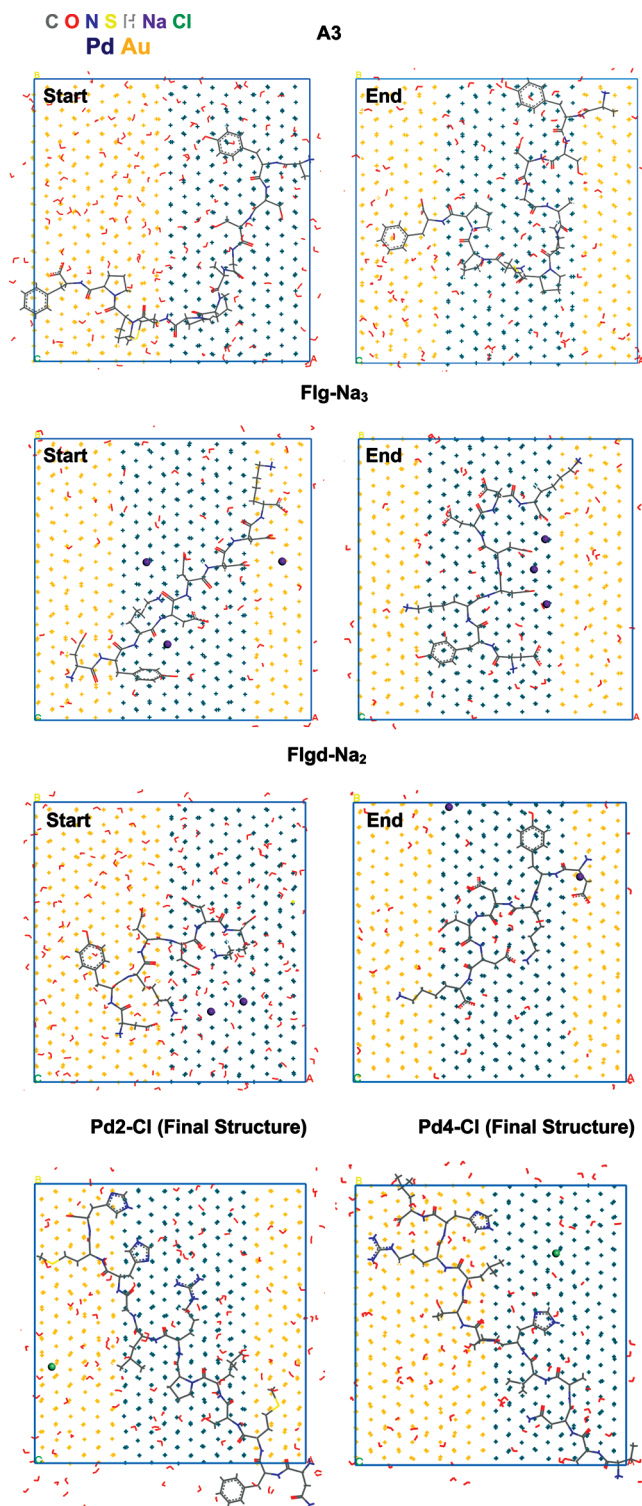
Figure 6. Representative snapshots of peptides on a Pd—Au {111} bimetal surface. A preference for Pd domains, the orientation of polar functional groups along the $Pd^{+0.3}\cdots Au^{-0.3}$ interface, and the position of residues on the hexagonal surface can be seen. Water molecules are partially shown to indicate the presence of solvent and maintain a clear view. The motion of larger peptides is restrained by finite box size.

adsorption of metal nanoparticles, and metallic double-helical structures were obtained. This observation coincides well with the strong attraction of aromatic side chains to both Au {111} and Pd {111} surfaces in the simulation (Tables 2 and 4). Fu et al. also mention the common adsorption of anionic groups such as CO_2^- on colloidal metal nanoparticles. This observation

concurs with the binding of Asp side chains in Flg—Na_3 and Flgd—Na_2 to Au {111} and Pd {111} surfaces, and possibly the proximity of the Asp side chains to Au {100} and Pd {100} surfaces in the simulation (Tables 2 and 4).

However, measurements of the adsorption energy of individual amino acids and peptides have yet rarely been reported. Li et al. measured the adsorption energy of pure acetic acid on Au—Pd {111} alloy surfaces by temperature-programmed desorption and reflection—absorption infrared spectroscopy.[20] While a quantitative comparison to aqueous solution is not possible, acetic is similar to Asp side chains in the Flg—Na_3 and Flgd—Na_2 peptides, or to Gly in protic environment. When the mole fraction of Au is greater than 0.5 in the bimetal, acetic acid adsorbs and desorbs reversibly with ~12 kcal/mol. When the Au fraction is below 0.33, acetic acid coordinates as an η^2 ligand at room temperature or decomposes on the surface.[20] The measured adsorption energy is qualitatively consistent with computed adsorption energies for Flg—Na_3 and Flgd—Na_2 peptides in water solution on the Pd—Au {111} surface (Table 4): approximately 4—5 CO_2^- groups coordinate to the surface, which would amount to 48—60 kcal/mol according to Li et al.; additional adsorption strength is gained through the Tyr residue and the peptide backbone which accounts for the total computed adsorption energy of 45—85 kcal/mol (Table 4). We have also seen a tendency toward η^2 coordination of the Asp side chains on Pd {111} surfaces in the simulation (Figures 4 and 6) in agreement with observations for pure acetic acid.[20]

The interaction of peptides with Ag, Au,[7,8] and Pd[8] salt solutions was investigated by Slocik et al. A3 and Flg—Na_3 reduce HAuCl$_4$, possibly through oxidation of the $_2$Tyr residue, and attach to the surface of the emerging metal nanoparticle with thermodynamically stable {111} faces[32—34,55] under non-oxidative conditions.[56,57] On the surface of the Au nanoparticles, A3 leads to a nanoparticle solution and Flg—Na_3 to nanoparticle precipitation. The average size (~diameter) of the fcc nanocrystalline Au particles of ~13 nm resulted in a narrow size distribution when the surface was covered with A3 and a wider size distribution of irregularly shaped particles when covered with Flg—Na_3. Simulation shows a clear preference for adsorption onto Au {111} surfaces over Au {100} surfaces, with adsorption energies of −63 and −63 kcal/mol compared to −9 and 0 kcal/mol for A3 and Flg—Na_3, respectively (Table 2). The peptides of 2.0—3.5 nm length are also small in relation to ~13 nm diameter of the grown particles, so an assumption of even surfaces (neglect of curvature) in the simulation may be acceptable. Separately, the peptides were incubated with Au nanoparticles of 30 nm diameter, and fluorescence measurements of $_2$Tyr (emission 303 nm) indicated a stronger relative adsorption of A3 vs Flg—Na_3 of 6.8 vs 5.1 with an uncertainty of 0.4 unit.[7] The simulation indicates equal values; however, adsorption of the longer A3 peptide could be slightly underestimated due finite size effects in the comparatively small simulation box. The difference between dispersion of A3-derived nanoparticles and precipitation of Flg—Na_3-derived nanoparticles appears to be related to different charge states, in addition to differences in adsorption energy: A3-coated nanoparticles are neutral and Flg—Na_3 coated nanoparticles are significantly

(55) Buffat, P.-A.; Flueli, M.; Spycher, R.; Stadelmann, P.; Borel, J.-P. *Faraday Discuss.* **1991**, *92*, 173–187.
(56) Wiley, B.; Sun, Y.-G.; Chen, J.-Y.; Cang, H.; Li, Z.-Y.; Li, X.-D.; Xia, Y. *MRS Bull.* **2005**, *30*, 356–361.
(57) Murphy, C. J.; Sau, T. K.; Gole, A. M.; Orendorff, C. J.; Gao, J.-X.; Gou, L.-F.; Hunyadi, S. E.; Li, T. *J. Phys. Chem. B* **2005**, *109*, 13857–13870.
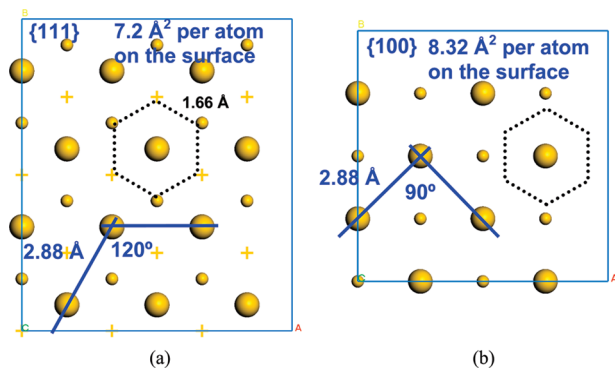
Figure 7. Comparison of the geometry (a) of the {111} surface and (b) of the {100} surface with numerical values for Au. The surface atomic layer is represented by spheres and subjacent repeat layers as smaller spheres and crosses. Dotted black lines indicate energetically favorable orientations of aromatic rings such as in Tyr, Phe, and Trp. In (a), the ring or a sp^2-hybridized group can occupy free fcc "lattice" sites, which contributes to high binding strength. In (b), complementarity to chain molecules is difficult to achieve so that small, flexible solvent molecules and possibly designed molecules with a rectangular repeat are of higher binding strength.

charged ($-3e$ per peptide plus 3 cations), which supports precipitation as a result of high local ionic concentrations. Infrared spectra of the peptides in solution and on the surface exhibit characteristic changes in the amide N—H stretch, the amide C=O stretch, and CO_2^- symmetric stretch frequencies.[7] We surmise that the proximity of binding residues to the metal surface and rearrangements in the local environment of hydrogen bonds (Figures 3 and 4) account for these observations; however, the assignment of the superimposed vibration frequencies to molecular details in the simulation remains as a challenge.

Hybrid gold—palladium nanostructures were synthesized starting with Au nanoparticles decorated with fusion peptides Flg—Na₃—A3 and A3—Flg—Na₃ and peptide A3. Solutions of the decorated Au nanoparticles were exposed to a macroscopic Pd {111} substrate,[8] and the affinity to the Pd {111} surface decreased in the same order. The trend of stronger adsorption of the peptides to Pd {111} surfaces compared to that observed on Au {111} surfaces agrees with the simulation (Figure 7); however, it is unknown from experiment whether the N-terminal or the C-terminal of the fusion peptide remains attached to the Au {111} surface. The same trend in affinity of the Au nanoparticles coated with Flg—Na₃—A3, A3—Flg—Na₃, and A3 was observed toward Pd nanoparticles (~3 nm diameter) upon incubation with K_2PdCl_6 solution and reduction by $NaBH_4$.[8] The formation of extended bimetallic Pd—Au interfaces[8] also supports the attraction of certain peptides (A3) to bimetal interfaces (Table 4), although specific comparisons are not possible on the basis of available experimental data.

Willett et al.[17] studied the adsorption of 20 peptides, each comprised of 8–10 identical residues (similar to Gly10 and Pro10), with fluorescent tags at the N-terminus on various surfaces, including Au and Pd. Unfortunately, the nature of the surfaces is unknown, and thermodynamically preferred {111} surfaces were likely destroyed by application of a 4-min oxygen plasma etch in favor of {100} surfaces. After incubation with peptide solutions at pH = 7, the number of adhered peptides per surface area was determined from the fluorescence intensity after several washing cycles. Fluorescence signals may have been quenched in peptides with all-aromatic side chains (Tyr10, Phe10, etc.), so the interpretation of the data is quite speculative. Nevertheless, strong adsorption of some peptides on oxidized Al and silica surfaces was found, while adsorption

on Au and Pd surfaces was always less than 10% on a relative scale: on Au, Arg and Thr were shown to adsorb slightly, and on Pd, His, Thr, Tyr, and Trp adsorbed. Data from other groups[1,4,7,8] and simulation results leave no doubt that peptides strongly adsorb on Au {111} and Pd {111} surfaces, comparable to their adsorption on surfaces such as alumina and silica. The thoroughly weak adsorption of all peptides in Willett's study, therefore, suggests the presence of {100} surfaces on which the simulation only shows approximately 10% of the adsorption energy compared to that observed on {111} surfaces (Table 2). The approach of Tyr and Ser (similar to Thr) in A3 to Au {100} and Pd {100} surfaces was found in the simulation (Table 2).

5.2. Binding Mechanism. Overall, computed adsorption energies provide interesting trends (Tables 2 and 4) and are in a justified relationship with available experimental data. All peptides containing 8−12 amino acids, including the nonspecialized reference peptides Gly10 and Pro10, exhibit neutral or attractive interactions with gold and palladium surfaces in a gross range from 0 to −100 kcal/mol of peptide. These interactions are comparable to the strength of 0−30 hydrogen bonds and appear to be a reasonable order of magnitude for metal binding: stronger than van der Waals interactions and hydrogen bonds alone, and weaker than covalent interactions.[1] All residues or a subset of binding residues in each peptide are then in direct contact with the metal surface and account for most of the adsorption energy (Tables 2 and 4). The amount of attraction depends on the metal, the surface, the amino acid, changes in conformation, polarity of the surface (Pd−Au), polarization at the interface, covalent contributions to bonding, and other factors. Direct contact with the metal surface may thus not be enough for strong adsorption, such as for Flg−Na₃ on Au {100} and Pd {100} surfaces.

The marked differences between adsorption on {111} and {100} surfaces can be related to the geometry of the surface (Figure 7), in agreement with the energy model of the simulation (eq S1, Supporting Information). Adsorbed molecules are most strongly bound to the metal surface when they serve as an approximate extension of the fcc lattice. This is particularly evident on the {111} surface, where metal atoms in the surface plane arrange in a hexagonal lattice (Figure 7a). The lattice involves angles of 120° and projected interatomic distances of 1.66 Å for Au and 1.59 Å for Pd in the two atomic layers below the surface atomic plane which create "free" fcc lattice positions above the metal surface with maximum van der Waals (metal-bonding) interactions. Therefore, adsorbed aromatic rings and extended sp^2-hybridized structures with bond angles of 120° and bond lengths of ~1.41 Å fit reasonably well on top of the surface. The density of surface atoms per unit area is also slightly higher on the {111} surface than on the {100} surface. On the other side, the {100} surface with angles of 90° and a projected spacing between "empty" fcc lattice sites of 2.88 Å for Au and of 2.75 Å for Pd is much less complementary to common sp^2- or sp^3-hybridized peptide chains or other organic molecules (Figure 7b). This quadratic pattern of available fcc lattice sites induces a significant mismatch to usual bond lengths and bond angles, which makes it difficult to bind peptides or other chain molecules to {100} surfaces. Instead, small, mobile water molecules are preferentially adsorbed and lead to small adsorption energies for all peptides on {100} surfaces (Table 2). In summary, aromatic residues, sp^2-configured groups such as CO_2^- of Asp, and sp^3-hybridized alkyl chains with tetrahedral bond angles of 109° and bond lengths of 1.54 Å are thus a better fit to {111} surfaces compared to {100} surfaces (Figures 3, 4,

and 6), and the compatibility with angles and spacing between available lattice sites can be exploited to design strongly or weakly binding peptides.

The nature of noncovalent binding of peptides and organic molecules to metal surfaces may thus be described as a soft epitaxy driven by complementarity to "empty" lattice positions. Yet bound molecules possess significant translational freedom compared to atoms in the metal surface plane, so several factors contribute to binding strength: (1) the interaction strength of the metal, proportional to its surface energy; (2) the interaction strength of the peptide or individual residues and its complementarity to the metal surface; (3) the interaction strength of the solvent and its complementarity to the metal surface; and (4) entropic factors and changes in secondary structure upon adsorption. In addition, polarization of the metal surface adds an amount of attractive energy that would be similar on {111}, {100}, {110}, or other surfaces. Also, charge transfer is possible. Both of these effects will be less significant in the presence of a solvent (e.g., water) of polarity similar to or higher than that of the peptide; however, they may tune peptide adsorption on less attractive (e.g., {100}) surfaces.

The concept of soft epitaxy also suggests that peptide adsorption is not highly specific to individual amino acids but rather to the peptide as a whole, and this aids in understanding the self-assembly of larger structures, such as Met nanogratings on even Ag {111} surfaces.[12] Additional evidence for the proposed binding mechanism from earlier simulations is provided in section S3 of the Supporting Information.

It is also instructive to compare the noncovalent mechanism of peptide adsorption to the covalent-type adsorption of alkanethiols on Au surfaces.[14−16,58] The dissociation energy of strongly binding peptide groups such as CO_2^- (Asp) and PhOH (Tyr) is on the order of 10−20 kcal/mol (sections 3 and 4), which is similar to an estimated dissociation energy of 11.5 kcal/mol[58] of the Au−S(C_nH_{2n+1}) bond in thiols, although the value for thiols still remains uncertain. A major difference between peptides and thiols is that peptides (excluding Cys) spread out their interaction over a greater area and several functional groups, while alkanethiols lead to pinpoint interactions at the R−SH headgroup which induce locally strong covalent forces. Thus, alkanethiols are likely to support the formation of adatoms and vacancies during the reduction of precursor metal salts.[14,16] Besides, the high density of Au atoms on even surfaces (three Au atoms per thiol headgroup)[15] favors thiol binding when the local surface roughness (i.e., the effective surface area) is increased, while the soft epitaxial adsorption of peptides benefits from locally regular, complementary surfaces.

6. Conclusion

Using molecular dynamics simulation and the consistent valence force field with accurate extensions for fcc metals, we computed adsorption energies of strongly binding peptides identified by phage display (A3, Flg−Na₃, Pd2−Cl, Pd4−Cl) as well as control peptides (Flgd−Na₂, Gly10, Pro10) on {111} and {100} surfaces of Au and Pd and on Pd−Au {111} bimetal surfaces in aqueous solution. Adsorption energies range from 0 to −100 kcal/mol per peptide of 8−12 amino acids. Strongly binding peptides often assume a flat-on 2D conformation so

that most residues are in direct contact with the metal surface, and weakly binding peptides retain more features of their preferred 3D conformation in solution so that layers of water molecules are present between the surface and a number of peptide residues.

A clear preference for adsorption to {111} surfaces over {100} surfaces is seen for all peptides in aqueous solution, which can be explained under consideration of available fcc lattice sites above the metal substrate. Above the {111} surface of Au and Pd, a hexagonal array of available lattice sites with a spacing near 1.60 Å can be favorably populated by aromatic rings or sp²-hybridized groups in the side chain or by the main chain of the peptide. On the other hand, a rectangular pattern of available lattice sites with a spacing of 2.88 Å above the {100} surface is more difficult to populate on time average by peptide molecules so that direct contact with small mobile water molecules is preferred. Besides, all peptides under consideration indicate a stronger adsorption on Pd {111} surfaces compared to Au {111} surfaces, which appears to be related to the higher surface tension and thus higher attraction to Pd {111} surfaces compared to Au {111} surfaces. Pd−Au {111} bimetallic surfaces also possess additional polarity, approximated by atomic charges of +0.3e and −0.3e at the Pd and Au sides of the interface, which influences the orientation of polar groups in the interfacial region, such as −C(=O)−NH− peptide bonds, NH_3^+ groups in Lys, or CO_2^- groups in Asp. Adsorption energies are found to be on the order of 10 kcal/mol higher (A3) and lower (Flg−Na₃) compared to those observed on the most attractive monometallic surface.

The concept of complementarity to available fcc lattice positions allows the distinction of strongly binding residues and less-binding residues. Strong adsorption on Au {111} and Pd {111} surfaces is particularly supported by aromatic and conjugated residues such as Tyr, Phe (preferably on Pd), His, Arg, Asp, and Asn, which can be regarded as "specific binding". However, strong adsorption also seems possible by less attractive residues such as Gly, Thr, Ser, and others. The binding is then enhanced through cooperative effects between many residues along the chain, e.g., Gly10, and may be regarded as "nonspecific binding".

The simulation approach presented is a first attempt to model metal interfaces with water and (bio)organic moieties using validated force fields,[24] explicit water models, and physically justifiable peptide concentrations (∼50 mM) at pH = 7 on a time scale of 10 ns. We employed a simple and efficient method to compute energies, free energies, and entropies of adsorption of solute molecules on a given surface that involves the simulation of four systems, the surface−solute−solvent system, the solute−solvent system, the solvent system, and the surface−solvent system, under consideration of equal molecular volumes of each component under NVT conditions. Limitations of the semiempirical classical simulation include the neglect of the explicit electronic structure, approximations in the energy model as well as a limited accuracy of the force field (particularly for water and peptides), and the neglect of polarization effects (of limited importance on even surfaces). Boltzmann averages of the sometimes strongly adsorbed peptides are challenging to obtain in spite of several independent start conformations, and the finite size of 3−5 nm in the 3D periodic model imposes a small but artificial symmetry restraint.

The results are intended as a first guide toward understanding the binding affinities of peptides to metal and bimetal surfaces, aiming at the design of peptides for specific surfaces. A range

(58) Dubois, L. H.; Zegarski, B. R.; Nuzzo, R. G. *J. Am. Chem. Soc.* **1990**, *112*, 570−579.
(59) Heinz, H.; Paul, W.; Binder, K. *Phys. Rev. E* **2005**, *72*, 066704.
(60) Heinz, H. *Mol. Sim.* **2007**, *33*, 747−758.

of experimental data supports the concept of dynamic epitaxy in solution and the description of binding versus less-binding residues, as well as computed binding energies in semiquantitative accuracy or better. Also, quantum-mechanical studies on peptide fragments support our view. Nevertheless, significant further insight could be obtained through further specific experimental characterization of binding constants and NMR data and through the exploration of the nanomechanical properties.[55,56] Other future challenges include the quantitative evaluation of the effects of curved and stepped surfaces, irregular surface structures, and the presence of ions on the binding of peptides, as well as testing of specifically synthesized molecules for complementarity to {111} and {100} surfaces.

Supporting Information Available: Background information on simulation methods (S1), a description of the computational screening approach (S2), simulation protocols (S3), and additional evidence on the binding mechanism from earlier simulations (S4). This material is available free of charge via the Internet at http://pubs.acs.org.

JA900531F